DESI Survey Validation Spectra Reveal an Increasing Fraction of Recently Quenched Galaxies at $z \sim 1$

David J. Setton,[1] Biprateep Dey,[1] Gourav Khullar,[1] Rachel Bezanson,[1] Jeffrey Newman,[1] Brett H. Andrews,[1] Arjun Dey,[2] Sarah Eftekharzadeh,[3] Stephanie Juneau,[2] Alan Pearl,[1] and Małgorzata Siudek[4, 5]

[1] Department of Physics and Astronomy and PITT PACC, University of Pittsburgh, Pittsburgh, PA 15260, USA
[2] NSF's NOIRLab, 950 N. Cherry Avenue, Tucson, AZ 85719, USA
[3] SOFIA Science Center, NASA Ames Research Center, Moffett Field, CA 94035, USA
[4] Institute of Space Sciences (ICE, CSIC), Campus UAB, Carrer de Magrans, 08193 Barcelona, Spain
[5] Institut de Física d'Altes Energies (IFAE), The Barcelona Institute of Science and Technology, 08193 Bellaterra (Barcelona), Spain

(Dated: November 1, 2022)

ABSTRACT

We utilize ~ 17000 bright Luminous Red Galaxies (LRGs) from the novel Dark Energy Spectroscopic Instrument Survey Validation spectroscopic sample, leveraging its deep (~ 2.5 hour/galaxy) spectra to characterize the contribution of recently quenched galaxies to the massive galaxy population at $0.4 < z < 1.3$. We use `Prospector` to infer non-parametric star formation histories and identify a significant population of young post-starburst galaxies that have joined the quiescent population within the past ~ 1 Gyr. This sample of recently quenched galaxies includes 277 at $z > 1$, which represents the largest spectroscopic sample of post-starburst galaxies at that epoch. At $0.4 < z < 0.8$, we measure the number density of quiescent LRGs, finding that recently quenched galaxies constitute a growing fraction of the total population with increasing lookback time. Finally, we quantify the importance of this population amongst massive ($\log(M_\star/M_\odot) > 11.2$) LRGs and explore the fraction of galaxies which formed a given proportion of their stellar mass in the Gyr before quenching. Although recently quenched galaxies are rare at $z \sim 0.4$ ($\lesssim 0.5\%$ of the population), by $z \sim 0.8$ the proportion of galaxies that formed $> 10\%$ of their stellar mass in the past Gyr grows to $\sim 3\%$. Relaxing this threshold, we find that galaxies with $f_{1\mathrm{Gyr}} > 5\%$ constitute $\sim 10\%$ of the massive galaxy population at $z \sim 0.8$ We also identify a small but significant sample of galaxies at $z = 1.1 - 1.3$ that formed $> 50\%$ of their stellar mass in the Gyr before quenching. Future analysis of this unprecedented sample promises to illuminate the physical mechanisms that drive the quenching of massive galaxies after cosmic noon.

Keywords: Post-starburst galaxies (2176), Galaxy quenching (2040), Galaxy evolution (594), Quenched galaxies (2016), Galaxies (573)

1. INTRODUCTION

In the local Universe, the vast majority of massive ($\log(M_\star/M_\odot) \gtrsim 11$) galaxies are completely quiescent and have been so for $5-10$ Gyr (e.g., Muzzin et al. 2013; Donnari et al. 2019; Leja et al. 2021). There is a growing consensus that two distinct pathways to quiescence are at play, with a rapid path dominating the buildup of quiescent galaxies at high redshifts and a slower channel that populates the "green valley" at low redshift (e.g.,

Wu et al. 2018; Maltby et al. 2018; Belli et al. 2019; Suess et al. 2021). The precise details of how the quiescent population grows from the rapid quenching pathway as a function of cosmic time remain very uncertain. Some studies have characterized the rates of rapid quenching as a function of cosmic time using either photometric (Whitaker et al. 2012; Wild et al. 2016; Belli et al. 2019; Park et al. 2022) or shallow spectroscopic (Rowlands et al. 2018) samples and have found that recently quenched galaxies, otherwise known as post-starburst galaxies, stopped contributing significantly to the quiescent population by $z \gtrsim 0.5$. However, photometric studies yield weak constraints on timescales. Thus, our

Corresponding author: David J. Setton
davidsetton@pitt.edu

picture of precisely when galaxies shut off their star formation and the contribution of late-time star formation remains poorly constrained.

Ideally, one would study the assembly of the red sequence by modeling the star-formation histories of complete samples of massive galaxies and studying how the incidence and characteristics of the population vary as a function of cosmic time. However, measuring the high-order moments of a star-formation history, such as timescales and burst fractions, requires high signal-to-noise continuum spectroscopy (Suess et al. 2022a). The limiting factor in performing such modeling has been the availability of spectra beyond $z \gtrsim 0.5$. The largest existing spectroscopic samples have not prioritized observing the gamut of quiescent galaxies; the SDSS LRG (Eisenstein et al. 2001) and BOSS (Dawson et al. 2013) surveys targeted the reddest quiescent galaxies, prioritizing pure, uniform samples at the expense of younger, bluer galaxies, and the EBOSS (Dawson et al. 2016) survey poorly sampled the quiescent population in favor of more accessible emission line sources. Deeper, more targeted surveys such as LEGA-C (van der Wel et al. 2021; Wu et al. 2018) and VANDELS (McLure et al. 2018; Carnall et al. 2019) have identified samples of ~1000s of massive quiescent galaxies at $z \gtrsim 0.5$, requiring significant investments on deep fields to reveal spectroscopic information for small samples.

The next generation of large spectroscopic surveys will revolutionize the availability of continuum spectroscopy of massive galaxies. The Dark Energy Spectroscopic Instrument (DESI) Survey (DESI Collaboration et al. 2016, 2022) is more than one year into its five year run and has already observed more galaxies than the entire Sloan Digital Sky Survey. Here we show that even the relatively small (~ 20000 galaxies) but deep Survey Validation 1 sample of Luminous Red Galaxies (LRGs) within the DESI Survey can be leveraged to identify new and exciting samples of recently quenched galaxies that push well beyond what previous surveys have been capable of (Zhou et al. 2022).

In this letter, we infer non-parametric star formation histories of LRGs in the DESI SV1 sample (Dawson et al. in preparation) and use them to study the growth of the red sequence from recently quenched galaxies. In Section 2, we describe the parent sample and demonstrate the use of non-parametric star formation histories to fit the spectrophotometric data with `Prospector` (Johnson & Leja 2017; Leja et al. 2017; Johnson et al. 2021). In Section 3, we use the results of this fitting to identify recently quenched galaxies and characterize their evolving number densities as a function of cosmic time. Finally, in Section 4, we discuss the implications

of these findings on our understanding of the physical mechanisms that are driving the production of massive, quiescent galaxies through the rapid quenching channel.

Throughout this letter, we use the terms "recently quenched galaxy" and "post-starburst galaxy" interchangeably to refer to galaxies which have recently and rapidly shut off their star formation. We assume a concordance ΛCDM cosmology with $\Omega_\Lambda = 0.7$, $\Omega_m = 0.3$ and $H_0 = 70 \mathrm{~km\,s^{-1}\,Mpc^{-1}}$, and quote AB magnitudes.

2. DATA

2.1. *The DESI LRG SV1 Sample*

In order to characterize the growth of the population of quiescent galaxies at intermediate redshifts, this work relies on the large program of deep spectra that were taken as a part of the DESI Survey Validation 1 (SV1) program (Dawson et al. in preparation). Over the course of its five-year lifetime, the DESI Survey will observe ~ 8 million luminous red galaxies with a well-understood selection function which can be used to construct a mass complete sample between $z = 0.4$ and $z = 0.8$ and which selects intrinsically bright galaxies out to $z \sim 1.5$ (Zhou et al. 2022). However, we restrict this study to the brightest SV1 LRGs with an observed fiber z magnitude $z_{\mathrm{fiber}} < 21.6$ cut similar to the one that is used in the full LRG sample. There are three primary reasons for this choice. First, the SV1 selection is significantly bluer than subsequent Survey Validation samples and the main DESI sample, which removes any potential bias against observing young, recently quenched LRGs. Second, the SV1 observations were an order of magnitude deeper than the observations for the main survey, with ~ 2.5 hours of integration per spectrum, resulting in the high signal-to-noise measurements of the continuum. Finally, by restricting to SV1 sample, the number of galaxies is computationally manageable and statistically large enough to make strong inferences about the galaxy population.

We select all tiles that were observed under the dark time observing conditions in SV1. We then select all galaxies which meet the LRG SV1 cuts outlined in Zhou et al. 2022 with an additional $z_{\mathrm{fiber}} < 21.6$ magnitude cut, a cut at $z > 0.4$ (above which the SV1 LRG sample begins to be mass complete), and a cut at $z < 1.3$ (at which point the H_δ absorption feature is no longer covered by DESI spectroscopy). We remove galaxies with poor redshift measurements by applying the cuts `DELTACHI2` > 25 and `ZWARN` $== 0$. These indicate that the redshift solution is not robust. We then remove the 580/17797 galaxies that did not reach target depth (exposure time $t_{\mathrm{exp}} > 1$ hour). The median exposure time of this final sample is 2.4 hours, with 16th and 84th
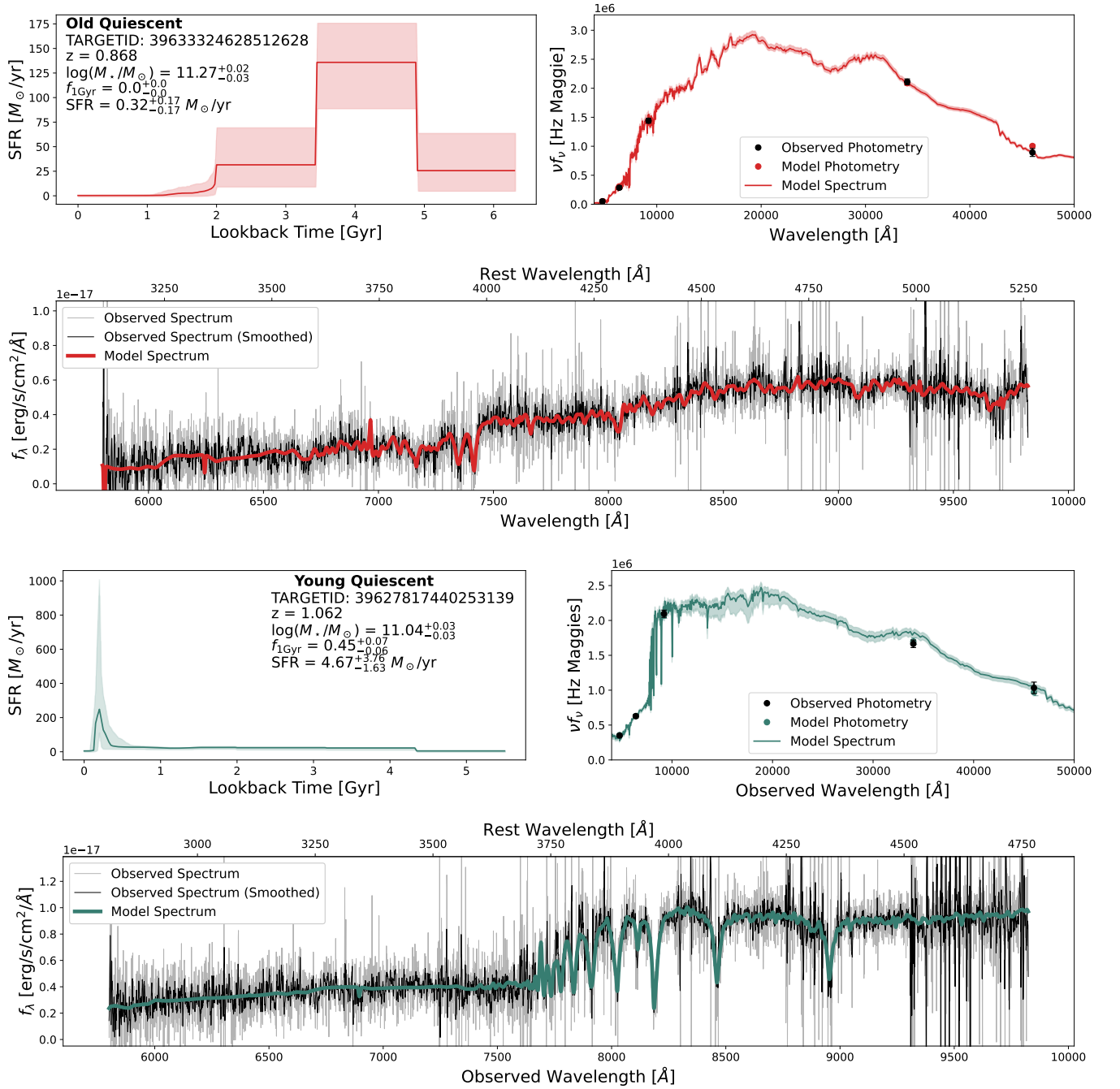
Figure 1. Example old (top, TARGETID=3963332462851262) and recently quenched (bottom, TARGETID=39627817440253139) galaxies from the DESI SV1 LRG Sample with `Prospector` fits using the star-formation history model from Suess et al. 2022a. For each galaxy, we show the median and 68% confidence interval star-formation history (top left) with selected galaxy properties. We also show the best fitting models (color) to the observed photometry ($g/r/z/W1/W2$, grey) (top right). Finally, we show the DESI spectrum (observed, grey; 5 pixel boxcar smoothed, black) along with the best fitting model (green) (bottom). From this modeling, we identify quiescent LRGs and infer the dominance of recent star formation and the timescale of quenching.

percentile exposure times of 1.5 and 4.1 hours respectively. This selection results in a total sample of 17217 galaxies. For each LRG, we compile the Milky Way extinction corrected $g/r/z/W1/W2$ photometry from the DESI Legacy Imaging Surveys DR9 (Dey et al. 2019, Schlegel et al. in preparation) and the "Fuji" internal data release which will be identical to the DESI Early Data Release (EDR, tentatively expected in early 2023).

2.2. Inferring Star Formation Histories with Prospector

We model the DESI spectra and photometry using non-parametric star formation histories with the SED fitting code Prospector (Johnson & Leja 2017; Leja et al. 2017; Johnson et al. 2021) to infer the detailed stellar populations of the sample. Non-parametric star-formation histories (SFHs) are particularly useful for fitting post-starburst galaxies because they do not impose an analytic form on the shape of the SFH, which allows for multiple rises and falls over the course of a galaxy's lifetime. We adopt a flexible bin model that is optimized to model recently quenching galaxies (Suess et al. 2022a). The model utilizes 3 fixed time bins at early times ($t_{\mathrm{lookback}} > 2$ Gyr), 5 flexible bins that each form the same amount of total stellar mass (allowing for greater resolution near periods of intense star-formation), and a final flex bin that allows a galaxy to remain quenched after star formation is finished. This scheme was extensively tested and is well designed to recover quenching timescales and burst mass fractions Suess et al. (2022a,b).

We use the dynesty dynamic nested sampling package (Speagle 2020), the Flexible Stellar Population Synthesis (FSPS) stellar population synthesis models (Conroy et al. 2009; Conroy & Gunn 2010), the MILES spectral library (Sánchez-Blázquez et al. 2006; Falcón-Barroso et al. 2011), and the MIST isochrones (Choi et al. 2016; Dotter 2016). We assume a Chabrier (2003) IMF and fix the model redshift to the spectroscopic redshift. In contrast with the Suess et al. 2022b prescription for fitting post-starburst galaxies, we elect to fit nebular emission non-physically by marginalizing over Gaussian lines at the locations of emission features in the spectrum. The massive LRG sample likely hosts many AGN which can contribute strongly to a galaxy's emission line strength (especially the recently quenched galaxies, e.g., Greene et al. 2020). Additionally, the LRG selection allows for the targeting of a small fraction of dusty star-forming galaxies with strong emission lines; we want to be completely agnostic to the source of emission when fitting star formation histories to these galaxies. We use the mass–metallicity prior described in Leja et al. (2019).

We utilize the PolySpecModel procedure which accounts for deviations between the shape of the photometry and the spectrum by dividing out a polynomial from the observed and model spectra during fitting. We assume the Kriek & Conroy (2013) dust law with a free A_v and dust index. Additionally, following Wild et al. (2020), we assume that the attenuation is doubled around young ($< 10^7$ yr) stars. We fix the shape of the IR SED following the Draine et al. (2007) dust emission templates, with $U_{\mathrm{min}} = 1.0$, $\gamma_e = 0.01$, and $q_{\mathrm{PAH}} = 2.0$. Finally, we include both a spectroscopic jitter term and the Prospector pixel outlier model. We center priors on the SFH such that they follow the predicted SFH of a massive quiescent galaxy from the Universe-Machine (Behroozi et al. 2019); this weakly prefers solutions with early-time star formation in the star formation histories we fit to ensure that outshining of a young stellar population is treated conservatively.

We fit all 17217 galaxies in the DESI SV1 LRG sample ($z_{\mathrm{fiber}} < 21.6$) with this procedure, providing the Milky Way extinction corrected $g/r/z/W1/W2$ photometry and the galaxy spectrum. Because the signal in the redshift range of interest is concentrated at the red end of the spectrograph, we elect to only fit the spectra from the R and Z arms of the spectrograph ($5800\text{Å} < \lambda_{\mathrm{obs}} < 9824\text{Å}$) to save on computation time and to avoid any issues with the flux calibration at the fainter end of the spectra. We note that the fits failed for 52/17217 galaxies (0.3% of the total sample). Visual inspection of the spectra of these failed fits suggests that they broadly fall into four categories: extremely low signal-to-noise galaxies, spectra with large masked regions, galaxies with incorrect redshift assignment, and broad-line AGN/QSOs (which our models are not equipped to characterize). As such, we omit the unmodeled galaxies and perform all analysis on the 17703 successfully fit galaxies.

Example fits to quiescent (top, red) and recently quenched (bottom, green) galaxies are shown in Figure 1. The quiescent galaxy that is representative of the majority of the DESI LRG sample is fit entirely with early star formation, consistent with a very old stellar population, and as such, all the mass was formed in the three fixed-width early-time bins. In contrast, the recently quenched galaxy is clearly fit with a post-starburst SED shape with strong Balmer absorption features and a characteristic lack of emission line infill. This indicates that the post-starburst galaxy has quenched after a period of intense star formation, and the star formation history reflects this. We infer that the galaxy began rapidly forming stars ~ 500 Myr before observation, and quenched ~ 150 Myr ago.
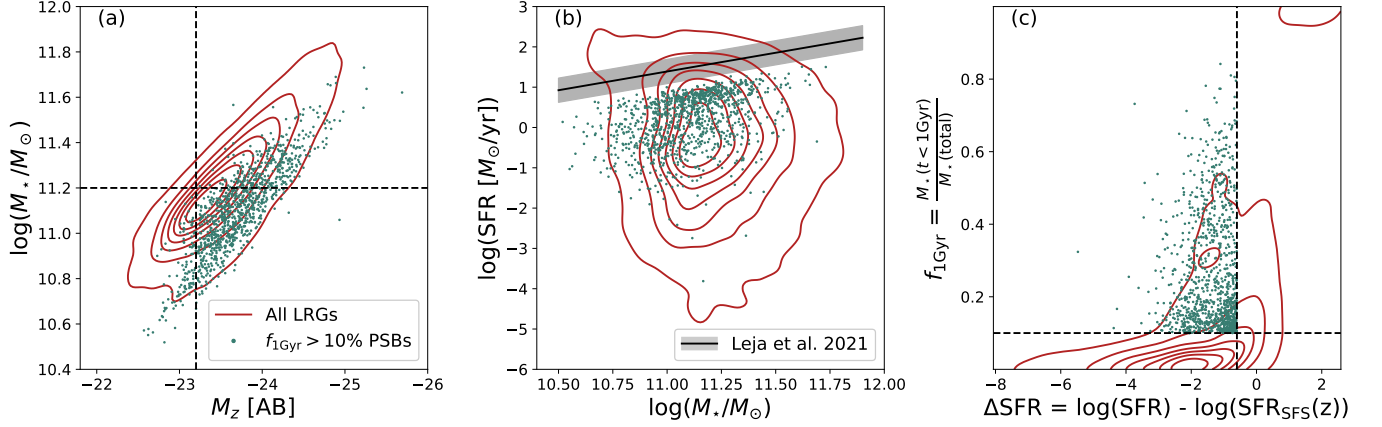
Figure 2. Properties of the full LRG sample (red contours) and a subset of post-starburst galaxies that recently quenched a significant episode of star formation using our fiducial selection ($f_{1\mathrm{Gyr}} > 0.1$, ΔSFR< -0.6, green points). In panel (a), we show the stellar mass versus the absolute magnitude (M_z) along with the magnitude limited threshold ($M_z < -23.2$) and the mass complete threshold ($\log(M_\star/M_\odot > 11.2$) discussed in Section 2.3. In panel (b), we show the star-formation rate versus stellar mass, with the star-forming sequence at $z = 0.7$, the median redshift of our sample, shown as a black line with characteristic ~ 0.3 dex 1σ scatter (Leja et al. 2021). In panel (c), we show the post-starburst selection plane, $f_{1\mathrm{Gyr}}$ versus ΔSFR, with the fiducial selection cuts illustrated as dashed lines. The post-starburst sample is significantly brighter than the parent sample at fixed stellar mass and occupies a unique part of parameter space by having formed a significant amount of recent stellar mass despite being fully quenched.

From the posteriors on the star formation histories, we derive a number of model parameters, many of which we directly use to select and characterize the properties of post-starburst galaxies. We measure the star-formation rate in all galaxies as the star-formation rate in the closest bin to the epoch of observation in the non-parametric star formation history. Above $\sim 1 M_\odot/\mathrm{yr}$, these star-formation rates have been shown to reliably recover the instantaneous star-formation rate of mock galaxies, and below this, they are effectively upper limits (Suess et al. 2022a). Additionally, quantify the offset from the star-forming sequence, ΔSFR, as:

$$\Delta\mathrm{SFR} = \log(\mathrm{SFR}) - \log(\mathrm{SFR_{SFS}}(z)) \qquad (1)$$

where $\mathrm{SFR_{SFS}}(z)$ is the inferred star formation rate from the star-forming sequence at the observed redshift of the galaxy defined in Leja et al. 2021, which is also measured using `Prospector` SED fits. We set a fiducial threshold for quiescence at ΔSFR $= -0.6$, $\sim 2\sigma$ below the main sequence at a given redshift. Finally, we measure the fraction of the total stellar mass formed in the Gyr before observation, $f_{1\mathrm{Gyr}}$.

We show some of the observed and derived characteristics of the full LRG sample as red contours in Figure 2. In the first panel, we show the stellar mass versus the rest frame absolute magnitude, M_z, illustrating the tight correlation between the two parameters. We additionally show lines which correspond to the cuts we make in the two parameters to construct the volume limited

samples described in Section 2.3. In the next panel, we show the star formation rate versus the stellar mass along with the "star forming sequence" at $z = 0.7$ with 0.3 dex scatter from Leja et al. 2021 to illustrate that the sample is largely quiescent. Finally, we show the sample in the post-starburst selection plane of $f_{1\mathrm{Gyr}}$ versus ΔSFR discussed in Section 3.1 with our fiducial cuts to select recently quenched galaxies. In all 3 planes, we show the fiducial sample of post-starburst galaxies as green points.

2.3. Selecting Volume Limited Samples

Because the choices made in spectroscopic targeting significantly impact the observed sample, it is necessary to select a volume limited sample to fairly compare galaxies across redshift bins. This is especially true because the $z_{\mathrm{fiber}} < 21.6$ cut in observed magnitude would observe a faint galaxy at low-redshift but not high-redshift. We use the fits to the spectrophometric data to select samples which we can use to infer number densities. Throughout this letter, we utilize three relevant samples: the full LRG sample, the rest absolute Z-magnitude selected "magnitude limited" sample, and the "mass complete" sample to select recently quenched galaxies. Here, we clarify those samples that we will refer to in this work.

By virtue of being the youngest and brightest galaxies in any given quiescent sample, post-starburst galaxies have the lowest $M_\star/L$ ratios at fixed stellar mass and therefore are relatively bright compared to the majority
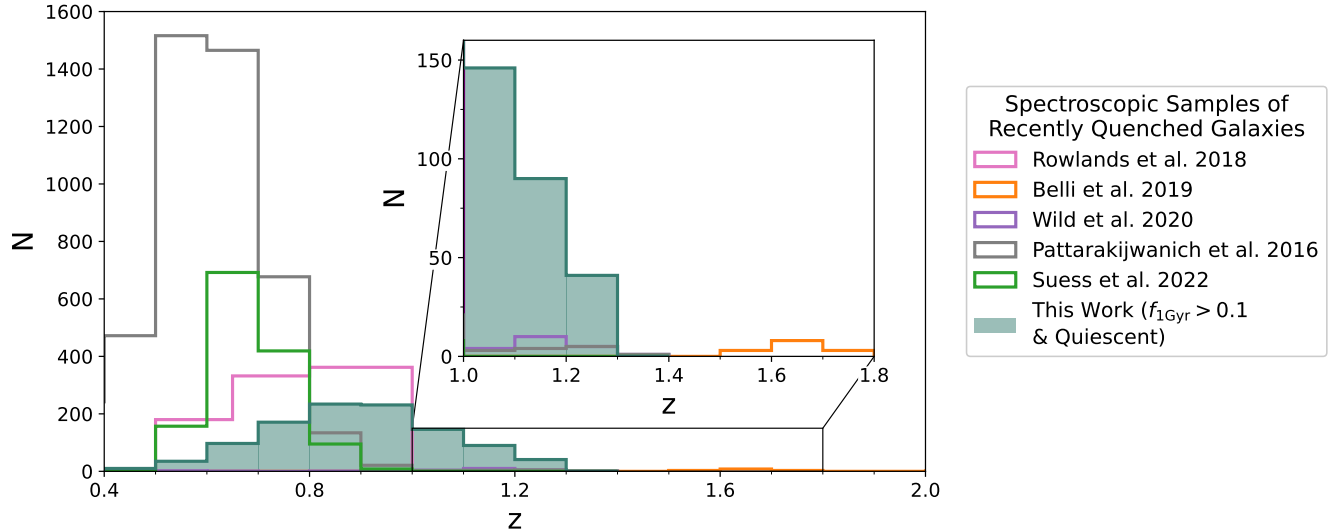
Figure 3. Redshift distributions of spectroscopic samples of recently quenched galaxies from $0.4 < z < 2.0$, with an inset focusing on $z > 1$ where the improvement in sample size from this work is most significant. Our fiducial post-starburst sample ($f_{1\mathrm{Gyr}} > 0.1$, $\Delta\mathrm{SFR} < -0.6$) is shown as a filled green histogram. Other samples shown include PCA-identified post-starburst galaxies from Rowlands et al. 2018 and Wild et al. 2020, galaxies with $t_{50} < 1.5$ Gyr from Belli et al. 2019, galaxies selected with K+A template fitting from the SDSS Pattarakijwanich et al. 2016, and galaxies selected using rest UBV filters from the SQuIGG$\vec{L}$E sample also selected from the SDSS (Suess et al. 2022b).

of LRGs. As such, in order to get large, complete samples of post-starburst galaxies to study as a function of redshift, a luminosity cut will maximize the sample size. We define a magnitude limited sample with rest-frame $M_z < -23.2$, at which the entirety of the reddest (in rest $g - z$ color) 2.5% of the LRG sample is selected at $z = 0.8$. This selection results in the largest volume limited sample we can obtain where we expect to have observed all bright post-starburst galaxies in DESI out to $z \sim 0.8$, yielding a total of 8683 galaxies.

While a magnitude limited sample is selects the bulk of the post-starburst galaxies in our sample, in order to characterize the growth of the post-starburst population relative to the fainter (at fixed stellar mass) old quiescent population, we also require a mass complete sample. In the redshift range $0.4 < z < 0.8$, the DESI LRG targeting only selects a sample which is $\gtrsim 80\%$ mass complete for very massive galaxies ($\log(M_\star/M_\odot)$ $\gtrsim 11.2$–accounting for systematic differences between the stellar masses we measure and those in Zhou et al. 2022). As such, in situations where we wish to compare to the quiescent population as a whole, we elect to use only galaxies above this stellar mass. This sample is significantly smaller than the magnitude limited sample, with only 5375 galaxies above the stellar mass cut at $z < 0.8$.

We show these cuts in Figure 2a, illustrating that the stellar mass cut is significantly more restrictive than the luminosity cut, which lets through post-starburst galax-

ies at masses as low as $10^{10.8} M_\odot$. At fixed stellar mass, the fiducial post-starburst sample (see Section 3.1) is significantly brighter than a typical LRG (red contours), and we therefore maximize our ability to constrain the number density of recently quenched galaxies as a population by instituting a cut on the absolute magnitude.

3. ANALYSIS

3.1. *Selecting Recently Quenched Galaxies*

There are a number of ways of selecting post-starburst galaxies, all of which share the common goal of selecting galaxies that recently quenched after a period of significant star formation. Historically, these galaxies have been selected using a combination of emission line cuts (to select against current star formation) and Balmer absorption depth (to select for a stellar population dominated by A type stars) (Dressler & Gunn 1983; Zabludoff et al. 1996; Balogh et al. 1999). Here, we leverage the tightly constrained star formation histories to select a physically motivated sample of recently quenched galaxies. First, we focus on selecting a pure quiescent sample. In Figure 2b+c, it is clear that some galaxies that are dusty and star-forming have been selected due to their red colors and exist in the LRG parent sample. To remove these, we perform a conservative cut in $\Delta\mathrm{SFR}$, classifying galaxies as quiescent only if their median $\Delta\mathrm{SFR}$ is $\sim 2\sigma$ (0.6 dex) below the star-forming sequence at their redshift from Leja et al. 2021. This selection, which is highlighted in Figure 2c, removes 2622

galaxies ($\sim 15\%$ of the total sample). All qualitative results in this work are insensitive to the exact definition of quiescence that we adopt, though exact sample sizes and number densities will by definition differ slightly.

Secondly, we are interested in separating the quiescent galaxy population physically into recent additions to the red sequence and older galaxies. In this work, our definition of recently quenched goes not require a burst, as we are interested in classifying all galaxies which rapidly formed a significant amount of stellar mass before quenching as post-starburst galaxies. To select such a sample, we leverage the inferred star formation histories to measure the fraction of the stellar mass formed within the last Gyr ($f_{1\mathrm{Gyr}}$) for all galaxies (see also Webb et al. 2020). In combination with the cut for quiescence, selecting galaxies with high $f_{1\mathrm{Gyr}}$ identifies a sample that must have rapidly truncated its star formation in order to have formed a large amount of its stellar mass while also reaching quiescence within 1 Gyr. We adopt $f_{1\mathrm{Gyr}} > 0.1$ (also shown in Figure 2c) for our fiducial post-starburst selection and explore the impact of different thresholds in Section 4. The fiducial selection identifies 1089 post-starburst galaxies from the 15012 quiescent LRGs using the fiducial $f_{1\mathrm{Gyr}} > 0.1$ selection.

This sample of post-starburst galaxies is unparelled in size beyond $z \gtrsim 1$. In Figure 3, we show the redshift distributions of this sample compared to other large spectroscopic samples of post-starburst galaxies at intermediate redshift. This sample of 100s of post-starburst galaxies at $z < 0.8$ is smaller than other samples which select galaxies from the full Sloan Digital Sky Survey (Pattarakijwanich et al. 2016; Suess et al. 2022b) or VIPERS Survey (Rowlands et al. 2018). However, at $z > 1$ (shown in the inset), we find that this sample dramatically increases the number of spectroscopically confirmed post-starburst galaxies at the tail end of cosmic noon.

While our selection of post-starburst galaxies relies on our inferred star formation histories, there are many other selections that use empirical measures of spectroscopic features to select post-starburst galaxies (French 2021). We choose a few common post-starburst identification methods and compare the resulting number densities with our fiducial model (see Section 3.2). For all literature comparisons, we use the same $\Delta\mathrm{SFR} \leq -0.6$ criterion for quiescence rather than relying on common empirical metrics like EW H_α, which falls out of our spectral window for most of the sample, or EW [OII], which is only a weak tracer of SFR due to contribution from AGN/LINERs. We note that while exact definitions of H_δ spectral indices vary in the literature (e.g., Alatalo et al. 2016 uses H_δ, French et al. 2015 uses $H_{\delta,A}$,

and Baron et al. 2022 $H_{\delta,F}$), these differences are subtle. We adopt $H_{\delta,A}$ as our preferred definition, as it is optimized for features from A-type stars (Worthey & Ottaviani 1997). The three selections we make are as follows:

1. $H_{\delta,A} > 4$ Å: After applying the quiescence criteria, we select 1727 galaxies with $H_{\delta,A} > 4$Å following e.g., French et al. 2015, 2018; Wu et al. 2018; Yesuf 2022.

2. $H_{\delta,A} > 5$ Å: We impose a more stringent cut, $H_{\delta,A} > 5$ Å, following e.g., Alatalo et al. 2016; Baron et al. 2022, selecting 1035 post-starburst galaxies.

3. SQuIGG$\vec{L}$E Selection: Finally, after applying the quiescence criteria, we use medium band synthetic rest-frame UBV filters to identify post-starburst galaxies with $U - B > 0.975$ and $-0.25 < B - V < 0.45$ following the procedure for selecting galaxies with SEDs dominated by A-type stellar populations (Suess et al. 2022b). We apply these cuts to the median best-fit models because the spectral coverage is not red enough to consistently overlap with the synthetic V filter. This selection finds only 324 post-starburst galaxies.

3.2. The number density of recently quenched galaxies

The DESI SV1 LRG selection is designed to have a uniform comoving number density of galaxies at $0.4 < z < 0.8$, which enables robust determination of number densities of subsets of the spectroscopic sample (Zhou et al. 2022). For this selection, we use the target density of 1439 deg^{-2} to calculate the number density in bins of $\Delta z = 0.1$ in redshift from $z = 0.4$ to $z = 1.3$ by measuring density of targets for a given selection criterion and dividing by the volume of the bin. We measure the number densities only for the magnitude limited or mass complete samples. We utilize jackknife resampling of the 31 SV1 pointings to calculate the errors on the measured number densities. The errors do not account for catastrophic redshift errors, but those should be very rare ($\leq 0.5\%$, see Zhou et al. 2022) and subdominant relative to cosmic variance and Poisson errors.

The comoving number density of each post-starburst sample as a function of redshift is shown in Figure 4. The raw number density of the DESI LRG SV1 sample ($z_{\mathrm{fiber}} < 21.6$) is shown in grey. We show the number density of the rest-frame magnitude limited ($M_z < -23.2$) sample with the fiducial quiescence cut ($\Delta\mathrm{SFR} < -0.6$) in red. We then apply the post-starburst selections outlined in Section 3.1 to the magnitude limited sample. The number densities are shown
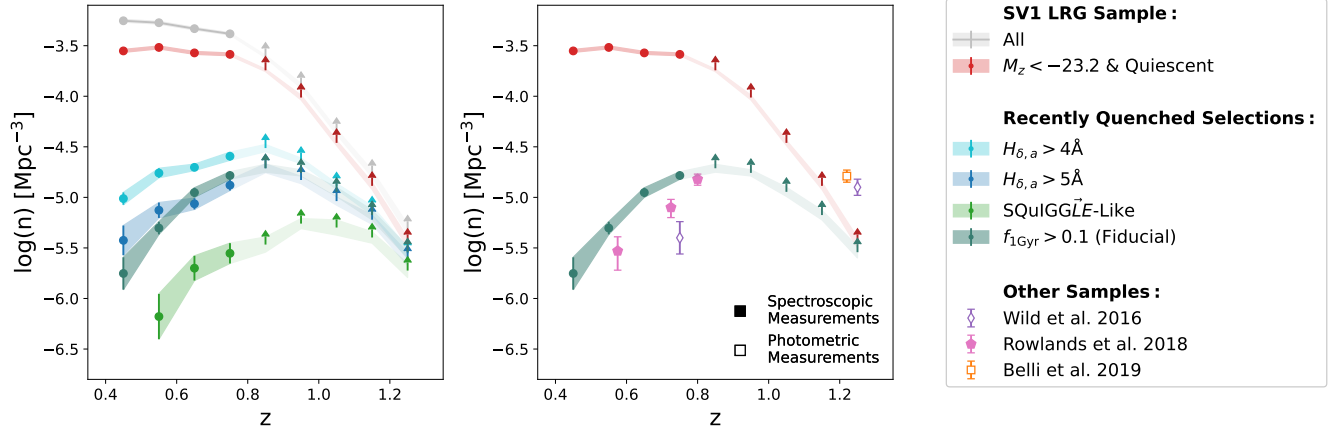
Figure 4. (Left): Number densities within the DESI SV1 LRG sample (full sample, gray; luminosity-complete and quiescent, red) and a variety of post-starburst selections from the luminosity-complete quiescent sample ($H_{\delta,a} > 4$, light blue; $H_{\delta,a} > 5$, dark blue; SQuIGG$\vec{L}$E SED selection, light green; and $f_{1\rm Gyr}$, green). Beyond $z \sim 0.8$, we indicate that the measured number densities are lower limits by plotting as upward facing arrows. All post-starburst selections show an increasing number density over the redshift range in which we are complete, with varying normalization resulting from the relative restrictiveness of the post-starburst criteria. (Right): The same magnitude limited LRG and $f_{1\rm Gyr} > 0.1$ samples as the previous panel in addition to literature measurements (photometric: open symbols; spectroscopic: filled symbols). All three of the Wild et al. 2016 ($M_\star > 10^{10.8} M_\odot$), Rowlands et al. 2018 ($M_\star > 10^{11} M_\odot$), and Belli et al. 2019 ($M_\star > 10^{10.8} M_\odot$) samples show a trend of increasing number density with redshift, but the normalization differs between the different samples as a result of differing stellar mass limits and selection techniques.

for $H_{\delta,A} > 4$ Å (light blue), for $H_{\delta,A} > 5$ Å (dark blue), SQuIGG$\vec{L}$E-like (light green), and our fiducial $f_{1\rm Gyr} > 0.1$ selection (dark green). In all cases, the number density of post-starburst galaxies rises as a function of redshift in the range of redshifts where the parent LRG sample is complete ($z < 0.8$). Above this, we illustrate that our measurements are lower limits.

In the second panel of Figure 4, we compare our fiducial sample of post-starburst galaxies to several measurements from the literature. We find qualitative agreement with previous studies (Wild et al. 2016; Rowlands et al. 2018; Belli et al. 2019). However, in detail, this comparison is limited by systematic effects; our sample is systematically more massive than other post-starburst samples, and is selected using above a magnitude (not mass) limit. Additionally, as shown in the first panel of Figure 4, differing identification techniques can significantly impact the measured number density of post-starburst galaxies. Still, a clear consensus emerges from this comparison that recently quenched galaxies are increasingly common at greater lookback time.

3.3. *Exploring the Growth of the Red Sequence by Rapidly Quenched Galaxies*

In the previous section, we studied the number density of a magnitude limited sample of post-starburst galaxies to maximize our sample size of post-starburst galaxies. Here, we attempt to quantify explicitly fraction of massive galaxies that have recently quenched and joined the red sequence as a function of cosmic time. To do so, we utilize the mass complete ($\log(M_\star/M_\odot) > 11.2$) subset of the LRG sample, which we show in first panel of Figure 5 (red) along with the corresponding stellar mass function from Leja et al. 2020. This measurement over-predicts the stellar mass function by ~ 0.2 dex at $z \sim 0.4$ while matching well at $z \sim 0.7$. This may be due to systematic differences in the stellar mass estimates (e.g., differences in modeled star formation histories, unmodeled contributions from AGN, or spectrophotometric modeling in our fits versus broadband multiwavelength SEDs), and the mismatch in redshift evolution may a result of the targeting incompleteness. As such, we adopt the number densities from the stellar mass function as the total abundance of of massive ($\log(M_\star/M_\odot) < 11.2$) galaxies and note that the fractions we measure may be systematically lower than reported by ~ 0.2 dex. Above $z = 0.8$ where LRG targeting is known to be incomplete, we inflate the upper error bar on the measured lower limits by assuming that every galaxy we have not targeted (quantified by the deviation between the measured number density and the stellar mass function) to capture the possibility that every galaxy we did not measure is a recently quenched galaxy. Since this is unlikely due to the lower $M_\star/L$ ratio of post-starburst galaxies, this conservative estimates captures the full range of possibility in the number density of galaxies in a given selection at $z > 0.8$.
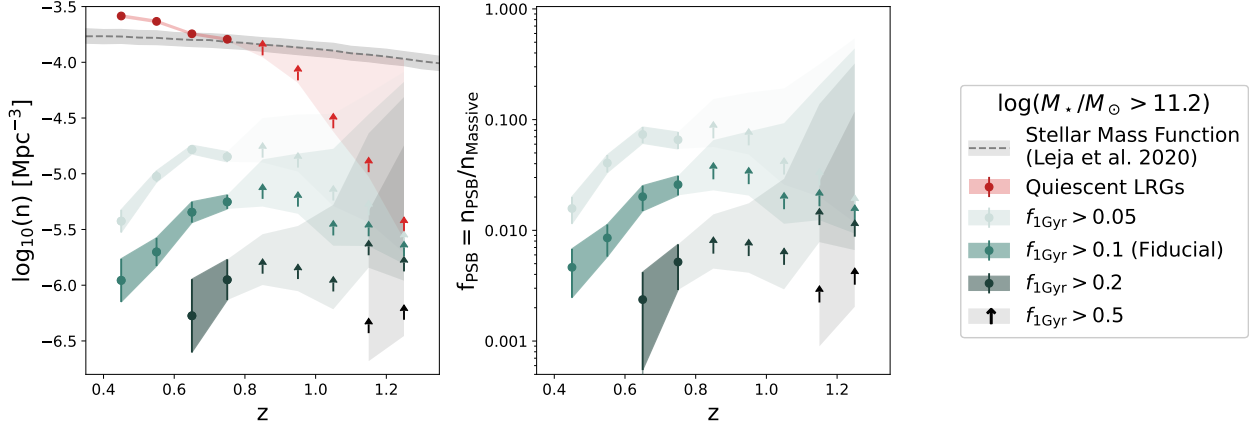
Figure 5. The number densities (left) and fractions (right) of recently quenched massive ($\log(M_\star/M_\odot) > 11.2$) galaxies. The dashed line and grey band (left) represent the stellar mass function of similarly mass galaxies (Leja et al. 2020), and the red points show the number density of all quiescent LRGs above the mass limit. The light green, green, dark green, and black points represent the number densities and fractions of recently quenched galaxies with $f_{1\mathrm{Gyr}}$ greater than 0.05, 0.1, 0.2, and 0.5 respectively. Above $z = 0.8$, measurements are indicated as lower limits with errors inflated to encapsulate the possibility that all galaxies which were not targeted by DESI meet the selection criterion.

We show the number densities of four different selections of recently quenched galaxies: $f_{1\mathrm{Gyr}} < 0.05$ (light green), $f_{1\mathrm{Gyr}} < 0.1$ (green), $f_{1\mathrm{Gyr}} < 0.2$ (dark green), and $f_{1\mathrm{Gyr}} < 0.5$ (black). Points that do not appear indicate that the redshift bin contained zero galaxies that met the selection criteria. All four sets of recently quenched galaxies show increasing number densities with redshift, but at $z \sim 0.8$, galaxies which formed a large fraction of their stellar mass in the past Gyr are very rare. For example, at $z = 0.8$, galaxies that formed $> 20\%$ of their stellar mass in the past Gyr were significantly (> 1 dex) rarer than those which formed 5% of their stellar mass. However, we find that the number density of the $f_{1\mathrm{Gyr}} > 20\%$ population cannot decreasing with lookback time, and in fact, at $z \sim 1.2$ the lower limit number density of this population is higher than the number density at z=0.8. The rarity of such objects at intermediate-z is extremely consistent with the rarity of "late bloomers," galaxies that formed the majority of their stellar mass in the 2 Gyr before quenching (Dressler et al. 2018). Additionally, we identify a very small population of galaxies which rapidly formed $\geq 50\%$ of their stellar mass in the Gyr before observation at $z = 1.1 - 1.3$, with lower limits that indicating a number density of at least $\log_{10}(\mathrm{n}) > -6.5$ Mpc^{-3}. Similar extreme post-starburst galaxies have been found in photometric samples and could represent analogs to the formation of massive quiescent galaxies at high-z (Park et al. 2022).

In the right panel of Figure 5, we show the same post-starburst samples as fractions of the total massive galaxy population (using the stellar mass function from Leja et al. 2020 as the denominator). We find that galaxies which formed $> 20\%$ of their stellar mass represent $\sim 0.5\%$ of the total galaxy population at z=0.8, but by $z \sim 1.2$ must be at least 1%, with an upper limit that extends to them being the entirety of the quiescent population. In contrast, galaxies with $f_{1\mathrm{Gyr}} > 5\%$ and $> 10\%$ are significant even at z=0.4, representing $\sim 1.5\%$ and 0.5% of the massive galaxy population, and by $z = 0.8$ they are $\sim 10\%$ and 3% of the total population. The general rarity of extreme post-starburst galaxies in this massive sample is consistent with findings that the formation redshift of $\log(M_\star/M_\odot) = 11.2$ galaxies is $z_{\mathrm{form}} \sim 2 - 3$ (Gallazzi et al. 2014; Pacifici et al. 2016; Fumagalli et al. 2016; Carnall et al. 2019; Estrada-Carpenter et al. 2019; Díaz-García et al. 2019; Webb et al. 2020; Khullar et al. 2022); at the epochs we are probing, the average massive quiescent galaxy quenched long in the past. However, we find that a significant number of massive galaxies are still quenching well after cosmic noon ($z \sim 2$), and expect that with a more complete sample, at higher redshift the population dominated by recent star formation would become the norm.

4. DISCUSSION AND CONCLUSIONS

Using the DESI SV1 sample, we measure non-parametric star formation histories for a novel sample of Luminous Red Galaxies. We select physically motivated samples of post-starburst galaxies and leverage the well characterized parent sample to characterize the increasing number density of recently quenched galaxies with lookback time. We find the following:

1. The sample of quiescent galaxies which formed $>$ 10% of its stellar mass in the past Gyr represents a novel spectroscopic sample. The 277 galaxies we identify at $z > 1$ are an order of magnitude larger than previous samples (see Figure 3).

2. The number density of post-starburst galaxies rises steadily with redshift from $z = 0.4 - 0.8$ based on our model selection and empirical identification methods (see Figure 4).

3. The fraction of massive $(\log(M_\star/M_\odot) > 11.2)$ galaxies which have recently quenched their star formation and which formed $> 10\%$ of their stellar mass in the past Gyr rises in this redshift range from $\lesssim 0.5\%$ at z=0.4 to $\sim 3\%$ in at z=0.8 (see Figure 5). Furthermore, at $z > 1$, we find a significant emerging population that formed $> 20\%$ and $> 50\%$ of its stellar mass in the past Gyr.

Using these findings, we now speculate on the physical mechanism that is driving the rapid quenching in this sample of galaxies. One of the most compelling fast processes that could shut off star formation and produce post-starburst galaxies is mergers (e.g., Hopkins et al. 2008). After cosmic noon, simulations have found that many massive galaxies that quench do so via major mergers (e.g., Wellons et al. 2015), which funnel gas inward and induce a burst of star formation that rapidly shuts off. Indeed, many studies of post-starburst galaxies have found that merger features are more common in post-starburst systems (e.g., Pawlik et al. 2016; Sazonova et al. 2021; Ellison et al. 2022, Verrico et al. 2022 in preparation).

We estimate the relative frequency of major mergers using the Universe Machine (Behroozi et al. 2019) and find that 15% and 20% of $\log(M_\star/M_\odot) > 11.2$ galaxies, at $z = 0.4$ and $z = 0.8$ respectively, experienced a major merger ($M_{\star,2}/M_{\star,1} > 25\%$ in the progenitor galaxies in the merger tree) in the past Gyr. This rate is significantly higher than the the 0.5% and 3% fractions we find for our fidicual sample of recently quenched galaxies, and the merger fraction increases more slowly than the post-starburst fraction. Some of this difference may be driven by gas-poor major mergers between already quiescent systems or gas rich mergers that do not quench, and we conclude that it is plausible that every very massive galaxy that rapidly quenches between $0.4 < z < 0.8$ does so as a result of a major merger. However, at high-z, our our measured lower limits fall short of placing strong constraints.

Still, the high-z tail of our distribution promises to be a very powerful tool for studying rapid quenching. Prior to DESI, only a small number of spectroscopic continuum observations from surveys could be mined for post-starburst galaxies above $z \gtrsim 1$ (Wild et al. 2020), and often samples can only be obtained through targeted followup of photometrically identified sources (e.g., Belli et al. 2019). Even in the smallest (but highest signal-to-noise) subset of DESI LRG spectra, we have identified an order of magnitude more spectroscopically confirmed post-starburst galaxies than had been measured previously. Future work will leverage these star formation histories further to study trends using parameters such as the time since quenching (Suess et al. 2022b), which has been used in post-starburst populations to constrain the evolution of AGN incidence (Greene et al. 2020), sizes (Setton et al. 2022), molecular gas contents (Bezanson et al. 2022), and merger fractions (Verrico et al. submitted). Using the combination of the unique spectroscopically derived moments of the star formation history and ancillary data, we hope to place strong constraints on the mechanisms that drive the quenching of massive galaxies as close to cosmic noon as is currently possible. Future surveys, such as PFS (Greene et al. 2022) and MOONRISE (Maiolino et al. 2020) will extend wavelength coverage into the NIR, pushing farther in redshift to cosmic noon. In conjunction with this sample, comprehensive studies of the properties of post-starburst galaxies from $z = 0$ to $z = 2$ will paint a cohesive picture of the rapid quenching process and its role in producing the present-day quiescent population.

REFERENCES

Alatalo, K., Lisenfeld, U., Lanz, L., et al. 2016, ApJ, 827, 106, doi: 10.3847/0004-637X/827/2/106

Balogh, M. L., Morris, S. L., Yee, H. K. C., Carlberg, R. G., & Ellingson, E. 1999, ApJ, 527, 54, doi: 10.1086/308056

Baron, D., Netzer, H., Lutz, D., Prochaska, J. X., & Davies, R. I. 2022, MNRAS, 509, 4457, doi: 10.1093/mnras/stab3232

Behroozi, P., Wechsler, R. H., Hearin, A. P., & Conroy, C. 2019, MNRAS, 488, 3143, doi: 10.1093/mnras/stz1182

Belli, S., Newman, A. B., & Ellis, R. S. 2019, ApJ, 874, 17, doi: 10.3847/1538-4357/ab07af

Bezanson, R., Spilker, J. S., Suess, K. A., et al. 2022, ApJ, 925, 153, doi: 10.3847/1538-4357/ac3dfa

Carnall, A. C., McLure, R. J., Dunlop, J. S., et al. 2019, MNRAS, 490, 417, doi: 10.1093/mnras/stz2544

Chabrier, G. 2003, PASP, 115, 763, doi: 10.1086/376392

Choi, J., Dotter, A., Conroy, C., et al. 2016, ApJ, 823, 102, doi: 10.3847/0004-637X/823/2/102

Conroy, C., & Gunn, J. E. 2010, ApJ, 712, 833, doi: 10.1088/0004-637X/712/2/833

Conroy, C., Gunn, J. E., & White, M. 2009, ApJ, 699, 486, doi: 10.1088/0004-637X/699/1/486

Dawson, K. S., Schlegel, D. J., Ahn, C. P., et al. 2013, AJ, 145, 10, doi: 10.1088/0004-6256/145/1/10

Dawson, K. S., Kneib, J.-P., Percival, W. J., et al. 2016, AJ, 151, 44, doi: 10.3847/0004-6256/151/2/44

DESI Collaboration, Aghamousa, A., Aguilar, J., et al. 2016, arXiv:1611.00036. https://arxiv.org/abs/1611.00036

DESI Collaboration, Abareshi, B., Aguilar, J., et al. 2022, arXiv e-prints, arXiv:2205.10939. https://arxiv.org/abs/2205.10939

Dey, A., Schlegel, D. J., Lang, D., et al. 2019, AJ, 157, 168, doi: 10.3847/1538-3881/ab089d

Díaz-García, L. A., Cenarro, A. J., López-Sanjuan, C., et al. 2019, A&A, 631, A157, doi: 10.1051/0004-6361/201832882

Donnari, M., Pillepich, A., Nelson, D., et al. 2019, MNRAS, 485, 4817, doi: 10.1093/mnras/stz712

Dotter, A. 2016, ApJS, 222, 8, doi: 10.3847/0067-0049/222/1/8

Draine, B. T., Dale, D. A., Bendo, G., et al. 2007, ApJ, 663, 866, doi: 10.1086/518306

Dressler, A., & Gunn, J. E. 1983, ApJ, 270, 7, doi: 10.1086/161093

Dressler, A., Kelson, D. D., & Abramson, L. E. 2018, ApJ, 869, 152, doi: 10.3847/1538-4357/aaedbe

Eisenstein, D. J., Annis, J., Gunn, J. E., et al. 2001, AJ, 122, 2267, doi: 10.1086/323717

12

Ellison, S. L., Wilkinson, S., Woo, J., et al. 2022, arXiv e-prints, arXiv:2209.07613. https://arxiv.org/abs/2209.07613

Estrada-Carpenter, V., Papovich, C., Momcheva, I., et al. 2019, ApJ, 870, 133, doi: 10.3847/1538-4357/aaf22e

Falcón-Barroso, J., Sánchez-Blázquez, P., Vazdekis, A., et al. 2011, A&A, 532, A95, doi: 10.1051/0004-6361/201116842

French, K. D. 2021, PASP, 133, 072001, doi: 10.1088/1538-3873/ac0a59

French, K. D., Yang, Y., Zabludoff, A., et al. 2015, ApJ, 801, 1, doi: 10.1088/0004-637X/801/1/1

French, K. D., Yang, Y., Zabludoff, A. I., & Tremonti, C. A. 2018, ApJ, 862, 2, doi: 10.3847/1538-4357/aacb2d

Fumagalli, M., Franx, M., van Dokkum, P., et al. 2016, ApJ, 822, 1, doi: 10.3847/0004-637X/822/1/1

Gallazzi, A., Bell, E. F., Zibetti, S., Brinchmann, J., & Kelson, D. D. 2014, ApJ, 788, 72, doi: 10.1088/0004-637X/788/1/72

Greene, J., Bezanson, R., Ouchi, M., Silverman, J., & the PFS Galaxy Evolution Working Group. 2022, arXiv e-prints, arXiv:2206.14908. https://arxiv.org/abs/2206.14908

Greene, J. E., Setton, D., Bezanson, R., et al. 2020, ApJL, 899, L9, doi: 10.3847/2041-8213/aba534

Hopkins, P. F., Cox, T. J., Kereš, D., & Hernquist, L. 2008, ApJS, 175, 390, doi: 10.1086/524363

Johnson, B., & Leja, J. 2017, Bd-J/Prospector: Initial Release, v0.1, Zenodo, doi: 10.5281/zenodo.1116491

Johnson, B., Foreman-Mackey, D., Sick, J., et al. 2021, dfm/python-fsps: python-fsps v0.4.0, v0.4.0, Zenodo, doi: 10.5281/zenodo.4577191

Khullar, G., Bayliss, M. B., Gladders, M. D., et al. 2022, ApJ, 934, 177, doi: 10.3847/1538-4357/ac7c0c

Kriek, M., & Conroy, C. 2013, ApJL, 775, L16, doi: 10.1088/2041-8205/775/1/L16

Leja, J., Johnson, B. D., Conroy, C., van Dokkum, P. G., & Byler, N. 2017, ApJ, 837, 170, doi: 10.3847/1538-4357/aa5ffe

Leja, J., Speagle, J. S., Johnson, B. D., et al. 2020, ApJ, 893, 111, doi: 10.3847/1538-4357/ab7e27

Leja, J., Johnson, B. D., Conroy, C., et al. 2019, ApJ, 877, 140, doi: 10.3847/1538-4357/ab1d5a

Leja, J., Speagle, J. S., Ting, Y.-S., et al. 2021, arXiv e-prints, arXiv:2110.04314. https://arxiv.org/abs/2110.04314

Maiolino, R., Cirasuolo, M., Afonso, J., et al. 2020, The Messenger, 180, 24, doi: 10.18727/0722-6691/5197

Maltby, D. T., Almaini, O., Wild, V., et al. 2018, MNRAS, 480, 381, doi: 10.1093/mnras/sty1794

McLure, R. J., Pentericci, L., Cimatti, A., et al. 2018, MNRAS, 479, 25, doi: 10.1093/mnras/sty1213

Muzzin, A., Marchesini, D., Stefanon, M., et al. 2013, ApJ, 777, 18, doi: 10.1088/0004-637X/777/1/18

Pacifici, C., Kassin, S. A., Weiner, B. J., et al. 2016, ApJ, 832, 79, doi: 10.3847/0004-637X/832/1/79

Park, M., Belli, S., Conroy, C., et al. 2022, arXiv e-prints, arXiv:2210.03747. https://arxiv.org/abs/2210.03747

Pattarakijwanich, P., Strauss, M. A., Ho, S., & Ross, N. P. 2016, ApJ, 833, 19, doi: 10.3847/0004-637X/833/1/19

Pawlik, M. M., Wild, V., Walcher, C. J., et al. 2016, MNRAS, 456, 3032, doi: 10.1093/mnras/stv2878

Rowlands, K., Heckman, T., Wild, V., et al. 2018, MNRAS, 480, 2544, doi: 10.1093/mnras/sty1916

Sánchez-Blázquez, P., Peletier, R. F., Jiménez-Vicente, J., et al. 2006, MNRAS, 371, 703, doi: 10.1111/j.1365-2966.2006.10699.x

Sazonova, E., Alatalo, K., Rowlands, K., et al. 2021, ApJ, 919, 134, doi: 10.3847/1538-4357/ac0f7f

Setton, D. J., Verrico, M., Bezanson, R., et al. 2022, ApJ, 931, 51, doi: 10.3847/1538-4357/ac6096

Speagle, J. S. 2020, MNRAS, 493, 3132, doi: 10.1093/mnras/staa278

Suess, K. A., Kriek, M., Price, S. H., & Barro, G. 2021, ApJ, 915, 87, doi: 10.3847/1538-4357/abf1e4

Suess, K. A., Leja, J., Johnson, B. D., et al. 2022a, ApJ, 935, 146, doi: 10.3847/1538-4357/ac82b0

Suess, K. A., Kriek, M., Bezanson, R., et al. 2022b, ApJ, 926, 89, doi: 10.3847/1538-4357/ac404a

van der Wel, A., Bezanson, R., D'Eugenio, F., et al. 2021, ApJS, 256, 44, doi: 10.3847/1538-4365/ac1356

Webb, K., Balogh, M. L., Leja, J., et al. 2020, MNRAS, 498, 5317, doi: 10.1093/mnras/staa2752

Wellons, S., Torrey, P., Ma, C.-P., et al. 2015, MNRAS, 449, 361, doi: 10.1093/mnras/stv303

Whitaker, K. E., Kriek, M., van Dokkum, P. G., et al. 2012, ApJ, 745, 179, doi: 10.1088/0004-637X/745/2/179

Wild, V., Almaini, O., Dunlop, J., et al. 2016, MNRAS, 463, 832, doi: 10.1093/mnras/stw1996

Wild, V., Taj Aldeen, L., Carnall, A., et al. 2020, MNRAS, 494, 529, doi: 10.1093/mnras/staa674

Worthey, G., & Ottaviani, D. L. 1997, ApJS, 111, 377, doi: 10.1086/313021

Wu, P.-F., van der Wel, A., Bezanson, R., et al. 2018, ApJ, 868, 37, doi: 10.3847/1538-4357/aae822

Yesuf, H. M. 2022, arXiv e-prints, arXiv:2207.12844. https://arxiv.org/abs/2207.12844

Zabludoff, A. I., Zaritsky, D., Lin, H., et al. 1996, ApJ, 466, 104, doi: 10.1086/177495

Zhou, R., Dey, B., Newman, J. A., et al. 2022, arXiv
  e-prints, arXiv:2208.08515.
  https://arxiv.org/abs/2208.08515